

*Original Article*

# Study of Structural Properties of $\text{Co}_{1+x}\text{Zr}_x\text{Fe}_{2-2x}\text{O}_4$ Spinel Ferrite

Dr. Jairam B. Mote<sup>1</sup>, Dr. Pravin K. Gaikwad<sup>2</sup> 

<sup>1</sup>Department of Chemistry, Adarsh College, Omerga, Osmanabad, Maharashtra, INDIA  
[jbmote51172@gmail.com](mailto:jbmote51172@gmail.com)

<sup>2</sup>Department of Physics, Shri Chhatrapati Shivaji College, Osmanabad, Maharashtra, INDIA  
[drpkgaikwad@gmail.com](mailto:drpkgaikwad@gmail.com) <https://orcid.org/0000-0003-2869-6751>

Corresponding Author - [drpkgaikwad@gmail.com](mailto:drpkgaikwad@gmail.com)

DOI - <https://doi.org/10.55083/irjeas.2022.v11i01001>

© 2023 Jairam B. Mote, Dr. Pravin K. Gaikwad

This is an article under the CC-BY license. This is an open access article distributed under the Creative Commons Attribution License, which permits unrestricted use, distribution, and reproduction in any medium, provided the original work is properly cited. <https://creativecommons.org/licenses/by/4.0/>

Received: 17 November 2022; Received in revised form: 28 December 2022; Accepted: 19 February 2023

**Abstract** - Nanocrystalline  $\text{Co}_{1+x}\text{Zr}_x\text{Fe}_{2-2x}\text{O}_4$  with different compositions with  $x = 0.0, 0.1, 0.2, 0.3, 0.4, 0.5$  and  $x = 0.6$  were efficiently prepared by sol-gel self-combustion. Citric acid served as fuel and metal nitrates were AR grade. X-ray diffraction results showed that a single-phase cubic spinel structure was produced. The crystallite size, lattice constant, and X-ray density are all within the above limits. The crystallite size supports the nanocrystallinity of the material. Porosity increases because the bulk density is much lower than the X-ray density. The cation distribution results indicate that the cobalt ferrite sample has an inverse spinel structure, with  $\text{Zr}_{4+}$  ions occupying [B] positions exclusively and  $\text{Co}^{2+}$  and  $\text{Fe}^{3+}$  ions occupying tetrahedral (A) and octahedral [B] positions, respectively. indicates possession.

**Keywords** – Cobalt Ferrite, Sol-gel auto Combustion, Structural Properties

## 1. INTRODUCTION

Due to the high surface to volume ratio of nanosize spinel ferrites, which makes them helpful in the applications of field of imaging and treatment [5, 6], drug delivery [7], catalyst [8], etc., extensive study has been carried out on them in recent years. The accommodation of a range of cations at their interstitial sites, tetrahedral (A) and octahedral [B] sites, is what gives spinel ferrites their significant uses. To highlight variations in electrical and magnetic characteristics, the spinel lattice can additionally

integrate the divalent, trivalent, and tetravalent cation. The synthesis process, circumstances, and parameters as well as the nature and type of the substituent and the cation distribution all have an impact on the characteristics of ferrite materials [9]. All of these factors may be quite important in modifying the electrical and magnetic characteristics that are beneficial for the intended uses. The sol-gel auto combustion process is the most widely utilized wet chemical technique for the manufacture of nanoscale spinel ferrite. This approach is popular because it offers several benefits over other methods, including good

chemical homogeneity, low processing temperature, and the ability to adjust the size, morphology, and other characteristics of the particles. Cobalt ferrite, a cubic spinel ferrite [10], has become the most well-known of these magnetic nanoparticles because of its strong coercivity (Hc), moderate saturation magnetization (Ms) [11, 12], good chemical stability, and high mechanical hardness [13]. Divalent cations are often substituted to change the characteristics of cobalt ferrites [14, 15]. There haven't been many reports in the literature about the impact of substituting trivalent ions and tetravalent ions on the fundamental electrical and magnetic characteristics of cobalt ferrites. The structural, electrical, and magnetic characteristics of zirconium-substituted cobalt ferrite  $\text{Co}_{1+x}\text{Zr}_x\text{Fe}_{2-2x}\text{O}_4$  ( $x = 0.0, 0.1, 0.2, 0.3, 0.4, 0.5,$  and  $0.6$ ) were examined in the current work. Zirconium is mostly employed as a refractory and an opacifier, but due to its great corrosion resistance, it is also utilized in tiny amounts as an alloying agent. Additionally, it has uses in biomedicine [16]. Here, we present the structural characteristics of a cobalt ferrite system swapped with zirconium.

## 2. EXPERIMENTAL TECHNIQUES

**2.1. Synthesis:** Citric acid was used as a fuel in the sol-gel auto combustion process to create  $\text{Co}_{1+x}\text{Zr}_x\text{Fe}_{2-2x}\text{O}_4$  ( $x = 0.0, 0.1, 0.2, 0.3, 0.4, 0.5,$  and  $0.6$ ) nanoparticles. Cobalt nitrate ( $\text{Co}(\text{NO}_3)_2 \cdot 6\text{H}_2\text{O}$ ), zirconium nitrate ( $\text{ZrO}(\text{NO}_3)_2$ ), ferric nitrate ( $\text{Fe}(\text{NO}_3)_3 \cdot 9\text{H}_2\text{O}$ ) ( $\text{C}_6\text{H}_8\text{O}_7 \cdot \text{H}_2\text{O}$ ). Cobalt ferrite nanoparticles were created using just analytical-grade chemicals that were employed directly after being received. Metal nitrates were added to fuel (citric acid) in separate glass beakers in the ratio of 1:3 according to stoichiometry. These were thoroughly dissolved into distilled water after being agitated for 15 to 20 minutes. They were combined once they had fully dissolved. To get the solution's pH value closer to 7 and stabilize the nitrate-citric acid solution, ammonia was gradually added to the mixture. Then for 6 hours on a hot plate, the neutralized solution was continuously magnetically stirred. The temperature was increased further to 1200C after the production of sol-gel, an extremely viscous gel, in order to initiate the ignition of the dry gel and ultimately produce powder. The loose cobalt ferrite powder was ground for 30 minutes before being annealed in a muffle furnace for 6 hours at 600°C.

**2.2. Characterizations:** Zirconium replaced cobalt ferrite samples were created in the current work using the sol-gel auto combustion process, and they were then examined using X-ray diffraction. All of the samples' X-ray diffraction patterns were captured using a RegakuMiniflex II X-ray powder

diffractometer running at 40kV and 30mA. Using Cu-K radiation with a wavelength of 1.5406 nm, the diffraction pattern was observed in the 2 range of 200 to 800. From the X-ray diffraction examinations, many structural characteristics including lattice constant, hopping length, particle size, X-ray density, porosity, and cation distribution were estimated.

## 3. RESULT AND DISCUSSION

### 3.1 Structural Properties:

**X-ray diffraction:** The produced samples of the  $\text{Co}_{1+x}\text{Zr}_x\text{Fe}_{2-2x}\text{O}_4$  ( $x = 0.0, 0.1, 0.2, 0.3, 0.4, 0.5$  and  $0.6$ ) system were characterized using the X-ray diffraction method. The X-ray diffraction (XRD) patterns for the  $\text{Co}_{1+x}\text{Zr}_x\text{Fe}_{2-2x}\text{O}_4$  ( $x = 0.0, 0.1, 0.2, 0.3, 0.4, 0.5$  and  $0.6$ ) system are shown in Fig. 1. Each XRD pattern exhibits well defined reflections that are part of the cubic Spinel structure. Figure 1 shows the  $\text{Co}_{1+x}\text{Zr}_x\text{Fe}_{2-2x}\text{O}_4$  XRD pattern. The XRD pattern's reflection peaks were all indexed using Bragg's law. The cubic spinel structure of all the samples is shown by the presence of planes (220), (311), (222), (400), (422), (511) and (440) in the XRD pattern. It is also obvious that each and every reflection peak is strong and distinct. Since there were no impurity peaks seen, the samples are single-phase in nature.

#### Lattice constant

Using the usual relation, the Lattice constant (a) calculated for samples of zirconium-substituted cobalt ferrite.

$$a = d \left( \sqrt{h^2 + k^2 + l^2} \right) - 1$$

Where, (h k l) is Miller Indices; (d) is interplanar spacing.

Table 1 lists the calculated lattice constant values (a). Considering the replacement of zirconium for cobalt and ferrous in the current ferrite system, the lattice constant gradually increases. Figure 2 depicts the fluctuation of the lattice constant a function of zirconium content x. The ionic radii of the component ions  $\text{Zr}^{4+}$ ,  $\text{Co}^{2+}$ , and  $\text{Fe}^{3+}$  may be used to understand the rise in lattice constant with zirconium concentration x. In the present system,  $\text{Co}^{2+}$  and  $\text{Zr}^{4+}$  ions take the place of two  $\text{Fe}^{3+}$  ions. The ionic radii of  $\text{Co}^{2+}$  and  $\text{Zr}^{4+}$  are 0.82 and 0.72, respectively, which is much bigger than the ionic radius of two  $\text{Fe}^{3+}$  (0.64) ions. As a result, the current system's lattice constant rises. The change of the lattice constant with zirconium is comparable to what has been described before [17].

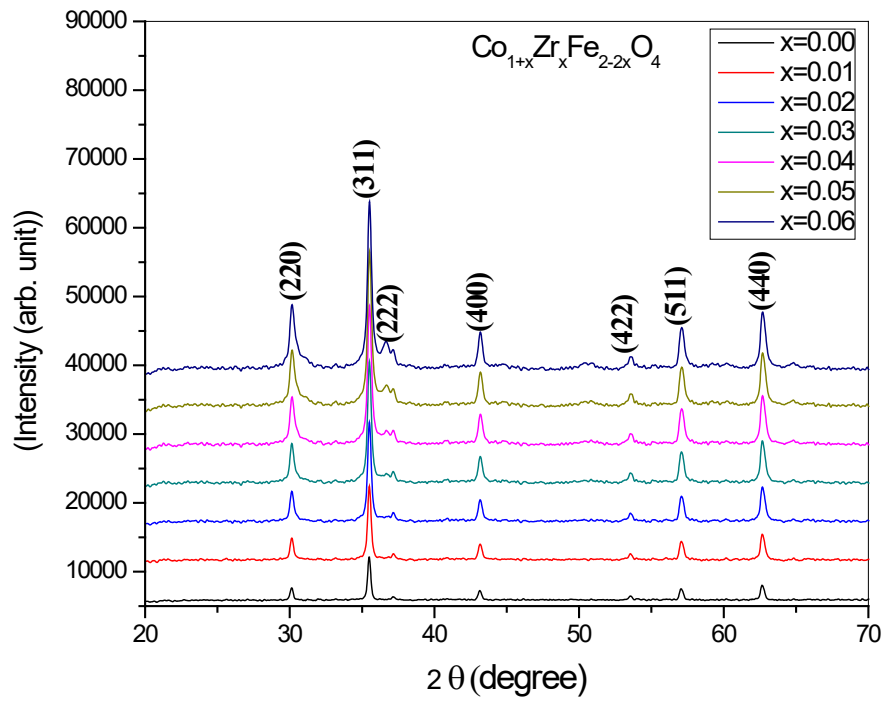


Fig.1: XRD pattern of  $Co_{1+x}Zr_xFe_{2-2x}O_4$

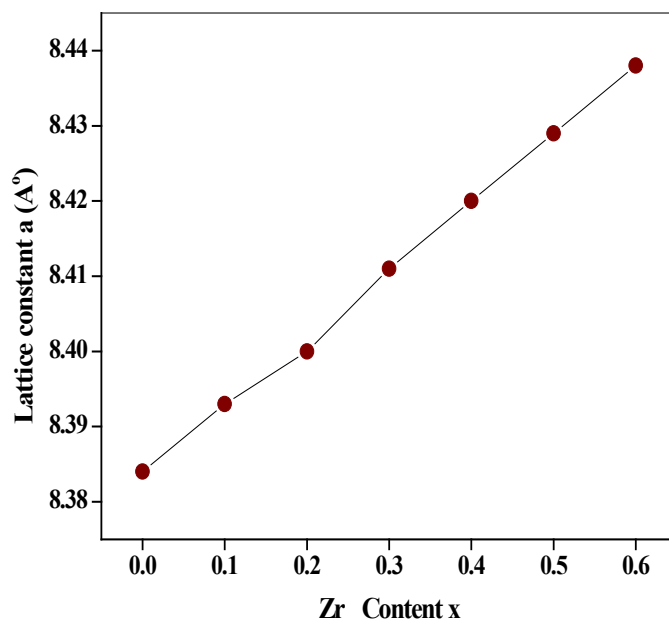


Fig.2: Variation of the ferrite system's lattice parameter "a" with respect to its Zr content "x"  $Co_{1+x}Zr_xFe_{2-2x}O_4$  (x = 0.00, 0.10, 0.20, 0.30, 0.40, 0.50 and 0.60)

**Unit cell volume:** The equation was used to compute the unit cell volume (V),

$$V = a^3 \tag{-2}$$

Where, a is the lattice constant; V is the unit cell volume.

With the replacement of zirconium for cobalt and ferrous in the current ferrite system, the unit cell volume (V) gradually increases. The rise in cell volume is related to an increase in the system's lattice constant.

**X-ray density:** The X-ray density (dX) was determined using the relationship, and the results are shown in Table 1.

$$d_X = \frac{ZM}{VN_A} \text{ gm/cm}^3 \tag{-3}$$

Where, N<sub>A</sub> is the Avogadro's number, Z is the number of molecules per unit, (Z = 8 for spinel system), M is molecular mass of the sample, V = a<sup>3</sup> is the unit cell volume.

Table 1 shows that as zirconium concentration of x increases, so does X-ray density. The rise in X-ray density might be a result of an increase in molecular weight / mass that outnumbers the increase in volume. Both unit cell volume and molecular weight grow in the current system. Figure 3 depicts the fluctuation of X-ray density with zirconium content x, which rises with increasing zirconium content x.

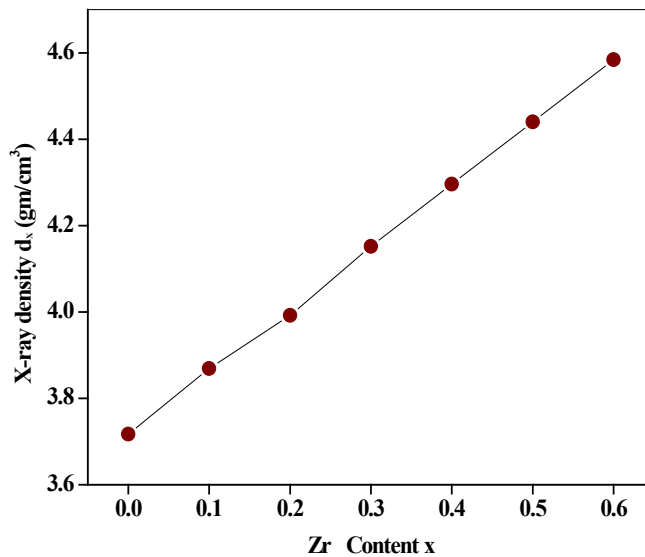


Fig. 3: Variation of the ferrite system's Zr content with respect to the X-ray density (dX)  $Co_{1-x}Zr_xFe_{2-2x}O_4$  (x = 0.00, 0.10, 0.20, 0.30, 0.40, 0.50 and 0.60)

**Bulk density**

Using toluene as an immersion solvent, the bulk density of the current sample has been calculated using the Archimedes principle. Table 1 displays the bulk density data. Table 1 shows that, like X-ray density, with increasing

zirconium concentration x, bulk density rises. The bulk density is observed to rise as the zirconium concentration of x increases. Fig.4 depicts the change in bulk density with zirconium content x.

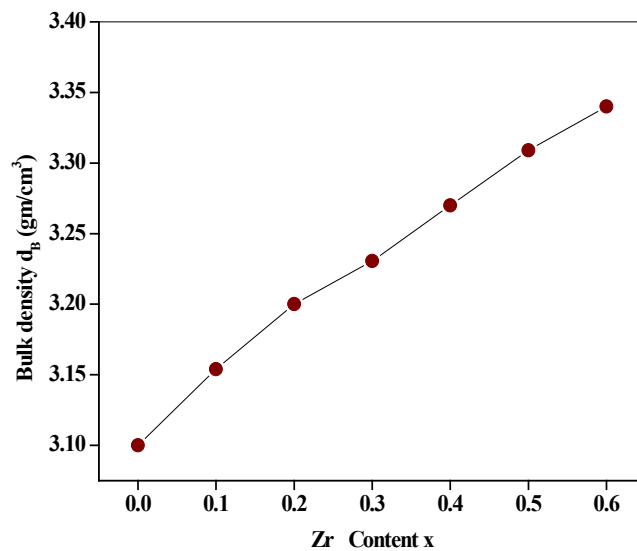


Fig.4: Variation of the ferrite system's bulk density ( $d_B$ ) with respect to Zr content ( $x$ )  $Co_{1+x}Zr_xFe_{2-2x}O_4$  ( $x= 0.0, 0.10, 0.20, 0.30, 0.40, 0.50, 0.60$ )

**Porosity**

By using the X-ray density ( $d_x$ ), the porosity ( $p$ ) and the bulk density ( $d_B$ ), of the zirconium replaced cobalt ferrite was calculated by the following equation:

$$P = 1 - \frac{d_B}{d_x} \%$$

-4

Figure 5 depicts the fluctuation of % porosity with regard to zirconium content  $x$ . The graph shows that zirconium content increases with percentage porosity  $x$ . The porosity of the current sample ranges between 16% to 26%.

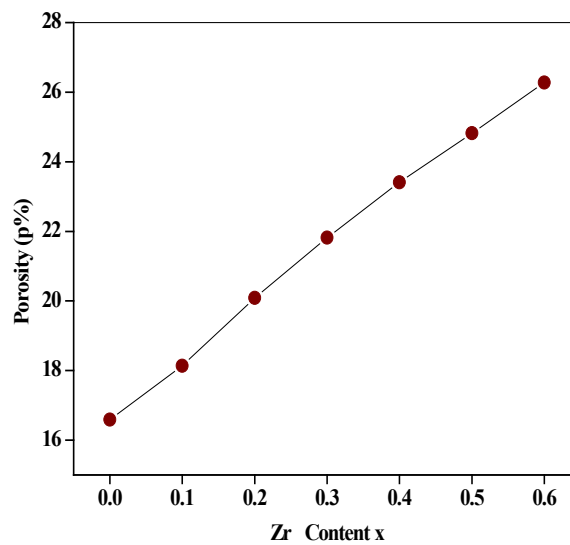


Fig. 5: Variation in the ferrite system's Zr content ( $x$ ) and percentage porosity ( $P\%$ )  $Co_{1+x}Zr_xFe_{2-2x}O_4$  ( $x = 0.00, 0.10, 0.20, 0.30, 0.40, 0.50, 0.60$ )

The obtained structural parameter values like bulk density, lattice constant, X-ray density,

percentage porosity and molecular weight are tabulated in Table 1.

Table 1: Bulk density ( $d_B$ ), X-ray density ( $d_x$ ), Lattice parameter ( $a$ ), Volume ( $V$ ), Porosity ( $P$  %), and Molecular weight of  $Co_{1+x}Zr_xFe_{2-2x}O_4$  system

Composition 'x'	A (Å)	$d_x$ (gm/cm <sup>3</sup> )	$d_B$ (gm/cm <sup>3</sup> )	P %	V (Å <sup>3</sup> )	Mol. wt. gm/mol
0.00	8.384	3.717	3.10	16.59	589.32	234.61
0.10	8.393	3.869	3.18	17.80	591.22	238.46
0.20	8.40	3.917	3.20	18.30	593.13	242.28
0.30	8.411	4.152	3.22	22.44	595.04	246.15
0.40	8.42	4.296	3.27	23.88	596.95	250.01
0.50	8.429	4.440	3.32	25.22	598.86	253.84
0.60	8.438	4.584	3.36	26.69	600.78	257.69

Using lattice constant values ( $a$ ), the various additional structural parameters such as tetrahedral bond length ( $d_{AX}$ ), hopping lengths ( $L_A$ ,  $L_B$ ), tetra edge ( $d_{AXE}$ ), octahedral bond length ( $d_{BX}$ ), and octaedge ( $d_{BXE}$ ) were determined for each sample using the conventional relations presented below. [18].

$$L_A = \frac{a\sqrt{3}}{4}$$

$$L_B = \frac{a\sqrt{2}}{4}$$

$$d_{AX} = a\sqrt{3}\left(u - \frac{1}{4}\right)$$

$$d_{BX} = a\left[3u^2 - \left(\frac{11}{4}\right)u + \left(\frac{43}{64}\right)\right]^{\frac{1}{2}}$$

$$d_{AXE} = \frac{a\sqrt{2}\left(2u - \frac{1}{2}\right)}{9}$$

$$d_{BXE} = \frac{a\sqrt{2}(1 - 2u)}{10}$$

$$d_{BXU} = \frac{a\left[4u^2 - 3u + \left(\frac{11}{16}\right)\right]^{\frac{1}{2}}}{11}$$

Table 2 shows the values of all of these structural characteristics. Because these characteristics are dependent on the lattice constant, their values increase as the zirconium content  $x$  increases. As the lattice constant of the current system grows, so do these properties.

Table 2: Hopping length ( $L_A$ ,  $L_B$ ), Octahedral bond ( $d_{BL}$ ), Tetrahedral bond ( $d_{AL}$ ), Tetra edge ( $d_{AE}$ ) and Octa edge ( $d_{BE}$ ) of  $Co_{1+x}Zr_xFe_{2-2x}O_4$  system

Composition 'x'	$L_A$ (Å)	$L_B$ (Å)	$d_{AL}$ (Å)	$d_{BL}$ (Å)	$d_{AE}$ (Å)	$d_{BE}$ (Å)	$L_A$ (Å)
0.00						Shared	Unshared
0.10	3.630	2.964	1.902	2.051	3.106	2.822	3.630
0.20	3.634	2.967	1.904	2.053	3.110	2.825	3.634
0.30	3.638	2.971	1.906	2.055	3.113	2.828	3.638
0.40	3.642	2.974	1.908	2.057	3.116	2.831	3.642
0.50	3.646	2.977	1.910	2.060	3.120	2.834	3.646
0.60	3.650	2.980	1.912	2.062	3.123	2.837	3.650

**Particle size**

Using the strongest peak (311), as well as the Debye-ratio Scherer's for small and uniformly sized cubic crystals [19], which is mentioned below, the zirconium substituting cobalt ferrite powders particle size was estimated.

$$t = \frac{0.9\lambda}{\beta \cos\theta} \text{ nm} \quad -12$$

Where,  $\lambda$  is wavelength of the Cu-K $\alpha$  radiation,

$\theta$  is Bragg's angle,

$\beta$  is the full width of the half maximum.

The obtained values of the particle size are presented in Table 3. The average particle size calculated by Debye Scherer's formula is of the order of 7 - 26 nm.

Table 3: Ionic radii ( $r_A$ ,  $r_B$ ) and Theoretical lattice parameter ( $a_{th}$ ) of  $Co_{1+x}Zr_xFe_{2-2x}O_4$  system

Composition 'x'	$r_A$ (Å)	$r_B$ (Å)	$a_{th}$ (Å)
0.00	0.582	0.726	8.360
0.10	0.584	0.728	8.414
0.20	0.586	0.730	8.440
0.30	0.588	0.732	8.470
0.40	0.590	0.734	8.510
0.50	0.592	0.737	8.540
0.60	0.595	0.739	8.570

**Tetrahedral ionic radius**

Using the oxygen positional parameter 'u' (u = 0.381) and the lattice constant value 'a', the tetrahedral A-site ionic radii may be determined as follows:

$$r_A = \left(u - \frac{1}{4}\right)a\sqrt{3} - r(O^{2-}) \text{ Å} \quad -13$$

Where,  $r_A$  represents radius of tetrahedral (A) site cation

$r(O)$ - represents radius of oxygen anions.

u- Oxygen positional parameter

**Theoretical lattice parameter**

The theoretical lattice parameter may be computed applying the subsequent relationship, which connects the Radius of cations component elements at the various lattice locations to the lattice parameter [20]:

Table 3 shows the tetrahedral ionic radius values, which rises with increasing zirconium concentration x. Ionic radius of octahedron The octahedral B-site ionic radii can use the equation to compute:

$$r_B = \left(\frac{5}{8} - u\right)a - r(O^{2-}) \quad -14$$

Where,  $r_B$  represents radius of octahedral [B] site cation

The values of octahedral ionic radius are given in Table 3 and It is discovered that it grows as the zirconium content x rises.

$$a_{th} = \left(\frac{8}{3\sqrt{3}}\right)(r_A + R_0) + \sqrt{3}(r_B + R_0) \quad -15$$

Where,  $r_A$  is tetrahedral site radius

$R_0$  is the radius of oxygen ion

$r_B$  is the octahedral site radius

Fig. 6 represents the variation of experimental and theoretical lattice constant as a function of zirconium content x.

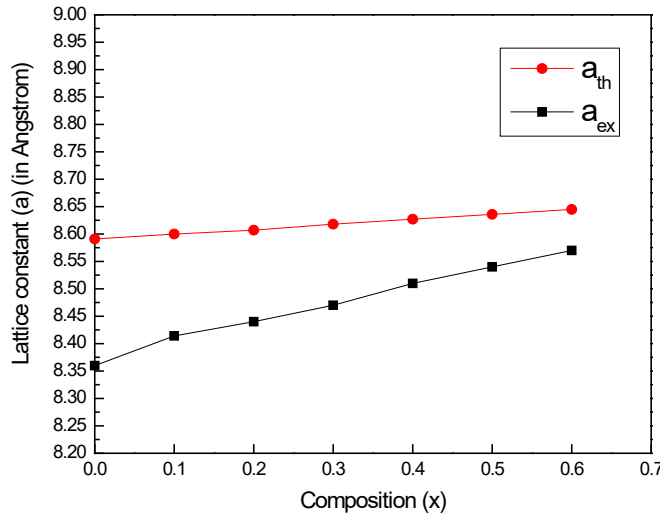


Fig. 6: Variation of experimental ( $a_{ex}$ ) & theoretical ( $a_{th}$ ) lattice Constant of  $Co_{1+x}Zr_xFe_{2-2x}O_4$  system

Figure 6 illustrates that the experimental and theoretical lattice constants have different values. The experimental and theoretical lattice

constants differ because theoretical the lattice constant was calculated using the hypothesized cation distribution, which is predicated on specific assumptions.

### CATION DISTRIBUTION

The distribution of cations in spinel ferrites may be determined using the XRD technique. Bertaut[21], Furuhashi et al.[22], and R-factor[23] present techniques for comparing experimentally observed and computed diffraction intensities for an extensive class of fictitious crystal structures. Neutron diffraction [24], electron spin resonance [25], nuclear magnetic resonance [26], thermoelectric method [27], and Mossbauer technique [28] may all be used to investigate the distribution of cations in spinel ferrites.

The cation distribution of the current system was determined using the Bertaut technique based on XRD in this study. In this method few pairs of reflections were selected which are sensitive to cation distribution and intensity of that reflection were calculated. Then the ratios were taken for the selected plane reflections. The computed and actual intensity ratios were

compared, and a distribution factor was included using expression [29].

$$R = \left| \frac{I_{obs}^{hkl}}{I_{obs}^{h'k'l'}} - \frac{I_{cal}^{hkl}}{I_{cal}^{h'k'l'}} \right|^{-16}$$

Where,  $I_{obs}^{hkl}$  the observed intensities for reflection (h k l)

$I_{obs}^{h'k'l'}$  the observed intensities for reflection (h'k'l')

$I_{cal}^{hkl}$  the calculated intensities for reflection (h k l)

$I_{cal}^{h'k'l'}$  the calculated intensities for reflection (h'k'l')

The observed and estimated intensity ratios are compared for various cation distributions at tetrahedral and octahedral sites based on their site preferences. The tiny value of the agreement factor (R) in this approach is a sign of the trustworthiness of the results and may be viewed as the system's probable cation distribution. This contains sensitive information on cation distribution is obtained by examining experimental and estimated intensity ratios for reflective surfaces whose values(i) are nearly entirely independent of the oxygen component, (ii) change rapidly with the cation distribution

in different directions, and (iii) do not differ substantially, the best information on cation distribution is obtained. The reflections that are most suited for cation distribution investigations are (220), (400), and (422).

Furthermore, for the determination of  $I_{cal}^{hkl}$ , a value of the oxygen parameter (u) must be assumed. Table 4 illustrates the estimated cation distribution for the current ferrites system.

Table 4: Cation distribution of  $Co_{1+x}Zr_xFe_{2-2x}O_4$  ( $x = 0.0, 0.1, 0.2, 0.3, 0.4, 0.5, 0.6$ ) System

Composition 'x'	Cation distribution	
	A-site	B-Site
0.00	$(Co_{0.05}Fe_{0.95})^A$	$[Co_{1.05}Fe_{0.95}]^B$
0.10	$(Co_{0.15}Fe_{0.85})^A$	$[Co_{1.05}Zr_{0.2}Fe_{0.75}]^B$
0.20	$(Co_{0.25}Fe_{0.75})^A$	$[Co_{1.05}Zr_{0.3}Fe_{0.65}]^B$
0.30	$(Co_{0.35}Fe_{0.65})^A$	$[Co_{1.05}Zr_{0.4}Fe_{0.55}]^B$
0.40	$(Co_{0.45}Fe_{0.55})^A$	$[Co_{1.05}Zr_{0.5}Fe_{0.45}]^B$
0.50	$(Co_{0.55}Fe_{0.45})^A$	$[Co_{1.05}Zr_{0.6}Fe_{0.35}]^B$
0.60	$(Co_{0.65}Fe_{0.35})^A$	$[Co_{1.05}Zr_{0.7}Fe_{0.25}]^B$

Table 4 shows that cobalt ions encircle octahedral (B) and tetrahedral (A) positions in all samples. Ferric ions were discovered to be distributed on both the octahedral [B] and tetrahedral (A) sites, whereas zirconium ions occupied exclusively the octahedral [B] sites.

The intensity ratios for the sensitive planes (220), (400), and (440) were computed using the cation distribution data (Table 4). Table 4 displays the observed and computed intensity ratio values.

Table 5: X-ray intensity ratios observed and calculated of  $Co_{1+x}Zr_xFe_{2-2x}O_4$  ( $x = 0.0, 0.1, 0.2, 0.3, 0.4, 0.5, 0.6$ ) system

Composition 'x'	I(220)/I(400)		I(220)/I(440)		I(400)/I(440)	
	Obs.	Cal.	Obs.	Cal.	Obs.	Cal.
0.00	1.12	1.33	0.22	0.21	0.532	0.459
0.10	1.31	1.35	0.70	0.61	0.53	0.45
0.20	1.17	1.36	0.74	0.62	0.64	0.46
0.30	2.39	1.37	1.002	0.63	0.42	0.46
0.40	2.17	1.38	1.17	0.63	0.54	0.45
0.50	3.40	1.39	1.64	0.63	0.48	0.46
0.60	2.26	1.41	1.52	0.65	0.67	0.46

The oxygen positioning parameter (u), octahedral site radius ( $r_B$ ), tetrahedral site radius ( $r_A$ ), and

theoretical lattice constant ( $a_{th}$ ) were computed from the cation distribution investigations and are

shown in Table 5. Theoretical lattice constants are discovered to be greater than experimental lattice constants. The mismatch in theoretical and experimental lattice constants might be attributed to inaccurate cation distribution data. This suggests

#### 4. CONCLUSION

The nanocrystal line  $\text{Co}_{1-x}\text{Zr}_x\text{Fe}_{2-2x}\text{O}_4$  with  $x=0.0, 0.1, 0.2, 0.3, 0.4, 0.5,$  and  $x = 0.6$  were successfully synthesized utilizing the sol-gel auto-combustion approach with metal nitrates of AR grade. The results of XRD revealed the creation of an isolated cubic spinel structure. The X-ray density, crystallite size, and lattice constant, are all within the previously reported

that the estimation of cation distribution using X-ray intensity computation must be modified. The table shows that the octahedral radius ( $r_B$ ) and tetrahedral radius ( $r_A$ ) rise as zirconium concentration  $x$  increases.

ranges. The crystallite size validates the materials nanocrystal line nature. X-ray density is less than the bulk density for this reason, porosity is enhanced. The cation distribution data show that  $\text{Fe}^{3+}$  and  $\text{Co}^{2+}$  ions encircle octahedral [B] and tetrahedral (A) sites, but  $\text{Zr}^{4+}$  ions encircle only the octahedral [B] site, suggesting that the cobalt ferrite sample has an inverse spinel structure.

#### REFERENCES

- [1] G.Kumar, J.Chand, S.Verma,M.Singh,J. Phys. D. Appl. Phys. 42, 155001-155006 (2009).
- [2] K.J.Standley, Oxide Magnetic Materials, Clarendon Press, Oxford, 1972.
- [3] G.B.Kadam, S.B.Shelke, K.M.Jadhav, J. Electro. Electri. Engg. 1(1) (2010) 15.
- [4] P. K. Gaikwad, S. S. Sawant and K. M. Jadhav J. Adv. App. Sci. Tech. Vol. 1. Issue 2 (2014) 35-37.
- [5] J.Gao, H.Gu, B.Xu, Acc.Chem.Res.42 (2009) 1097-1107.
- [6] M.Grigorova, H.J.Blythe, V.Blaskov, *etal.*J.Magn.Magn.Mater.183(1998) 163-172.
- [7] Wu H., G.Liu, X.Wang, J.Zhang, Y.Chenet *al.*, ActaBiomaterialia, 7 (2011) 3496-3504.
- [8] P.Lahiri, S.K.Sengupta, CAN. J. Chem. Vol. 69(1991) 33-36.
- [9] A.M.Shaikh, S.S.Bellad, B.K.Chougule, J. Magn. Magn. Mater. 195 (1999) 384.
- [10] M. Grigorova, H.J.Blythe, V.Blaskov, *et al.* J.Magn.Magn.Mater.183 (1998) 163-172.
- [11] L.J.Zhao, H.J.Zhang,Y.Xing, *etal.*, J. Solid State Chem.181 (2008) 245-252.
- [12] K.Maaz, ArifMumtaz, S.K.Hasanain, *et al.*, J. Magn. Magn. Mater. 308 (2007) 289-291.
- [13] D.Zhao, X.Wu, H.Guan, *et al.*,J.Supercrit.Fluids 42 (2007) 226-233.
- [14] S.G.Algude, S.M.Patange, S.E.Shirsath, D.R.Mane, K.M.Jadhav, J. Magn. Magn. Mater. 350 (2014) 39-41.
- [15] NallaSomaiah, Tanjore V. Jayaraman, P.A.Joy, Dibakar Das, J. Magn. Magn. Mater. 324:14 (2012) 2286-2291.
- [16] P. K. Gaikwad Int. J. of Eng. Res. and Adv. Dev. Vol. 4, Issue 01 Jan (2018) 58-63.
- [17] P. K. Gaikwad, S. S. Sawant Int. J. of Res. Thoughts Vol.10 Issue 01 Jan (2022)a585-a592.
- [18] S.E.Shirsath, B.G.Toksha, K.M.Jadhav, Mater. Chem. Phys. 117 (2009) 163.
- [19] Y.H.Hou, Y.J.Zhao, Z.W.Liu, H.Y.Yu, X.C.Zhong, W.Q.Qiu, D.C.Zeng, L.S.Wen, J. Phys. D, 43 (2010) No. 44, 445003.
- [20] S.Thankachan, B.P.Jacob, S.Xavier, E.M.Mohammed J. Magn. Magn. Mater. 348 (2013) 140-145.
- [21] L.Weil, E.F.Bertaut, L.Bochiro, J. Phys. Radium 11 (1950) 208.
- [22] H.Furuhashi, M.Inagaki, S.Naka, J. Inorg. Chem., 35(1973) 3009.
- [23] J.M.R.Gonzalez, C.O.Arean, J. Chem. Soc., Dalton Trans. (1985) 2155.
- [24] U.Schmockler, H.R.Boesch, F.Waldner, Phys. Lett. 40 A (3) (1972) 237.
- [25] C.C.Wu, T.O.Mason, J. Amer. Ceram. Soc., 64 (9) (1981) 520.

- [26] K.E.Sickafus, J.M.Wills, J. Amer. Ceram. Soc. 82(12) (1999) 329.
- [27] E.Stall, P.Fischer, W.Halg, G.Maier, J. Phys. Paris.25 (1964) 447.
- [28] Frauenfelder, H., The Mossbauer Effect, A Review with a Collection of Reprints (W. A. Benjamin, New York, 1963).
- [29] Qiang-Min Wei, Jian-Biao Li, Yong-Jun Chen, J. Mater. Sci. 36 (2001) 5115.

**Conflict of Interest Statement:** *The authors declare that there is no conflict of interest regarding the publication of this paper.*

*Copyright © 2023 Dr. Jairam B. Mote, Dr. Pravin K. Gaikwad. This is an open-access article distributed under the terms of the Creative Commons Attribution License (CC BY). The use, distribution or reproduction in other forums is permitted, provided the original author(s) and the copyright owner(s) are credited and that the original publication in this journal is cited, in accordance with accepted academic practice. No use, distribution or reproduction is permitted which does not comply with these terms.*

*This is an open access article under the CC-BY license.*

*Know more on licensing on*

<https://creativecommons.org/licenses/by/4.0/>

